Open access • Journal Article • DOI:10.1049/IET-GTD.2015.0601

Critical span identification model for dynamic thermal rating system placement

Jiashen Teh, Ian Cotton

Published on: 30 Nov 2015 - Iet Generation Transmission & Distribution (IET Digital Library)

Topics: Span (engineering)

IET Generation, Transmission & Distribution

Research Article

IET Journals
The Institution of Engineering and Technology

Critical span identification model for dynamic thermal rating system placement

ISSN 1751-8687
Received on 26th February 0000
Accepted on 31st July 2015
doi: 10.1049/iet-gtd.2015.0601
www.ietdl.org

Jiashen Teh ✉, *Ian Cotton*

Department of Electrical and Electronic Engineering, The University of Manchester, Oxford Road, Manchester, UK
✉ *E-mail: jiashen.teh-2@manchester.ac.uk*

Abstract: Dynamic thermal rating (DTR) system is one of the efficient ways to increase transmission lines utilisation. Ideally, its application requires the deployment of sensors on each span of the transmission line. This is because a transmission line normally traverses a large geographical area and is affected by various weather conditions. Consequently, each span elongates differently and has different thermal ratings from one another. However, due to the large number of spans, it is uneconomical to place sensors on each span. Whilst doing that, it is also vital to ensure that the DTRs do not cause overrating in any spans to the point of causing ground clearance infringement. Among these spans, some appear to have lower thermal capacity due to its undesirable surrounding weather conditions and may also have smaller ground clearances. In this study, these spans are known as the "critical span". This study proposed that by monitoring only these critical spans, the DTRs obtained can be safely applied to all other spans without the risk of ground clearance infringement. To do that, a novel critical span identification technique for the optimum placement of DTR sensors is presented in this paper.

1 Introduction

The demand for electricity has been rising at a rate faster than the expansion of transmission network capacity. This problem is further aggravated by political issues, environmental conservation movements and economic constraints that halt the expansion of transmission assets [1]. One of the reasons for inadequate transmission capacity is the usage of static thermal rating (STR), which largely underestimates the actual capacity of transmission lines by considering the worst sets of ambient weather conditions [2, 3]. Unlike STR, dynamic thermal rating (DTR) calculates line ratings according to actual weather conditions and allows full utilisation of transmission capacity [1, 4]. As a result, the new-found capacities can be exploited to satisfy more load points and reduce the need to increase transmission assets. Moreover, the cost of DTR is only a small fraction of that needed to invest in new lines or major physical upgrades [5–8]. Hence, migration from STR to DTR is beneficial.

However, implementation of DTR brings with it a set of challenges. In order to illustrate this, the normal scenario for transmission lines is explained. Transmission lines normally traverse a large geographical area and consist of many spans. Across this vast area, weather conditions change significantly and have different effects on the ratings and sagging levels of the spans. Too much sagging will violate ground clearance and may inflict harm on living species and valuable assets beneath. Overrating of spans will cause annealing and ageing to their conductors and lead to more sagging. On the other hand, underrating wastes a large portion of unused current-carrying capacity. Clearly, having accurate data on the weather affecting the spans is vital for optimising the line operating conditions. Therefore, ideally, the implementation of a DTR system requires the deployment of weather sensors along the transmission lines. However, it is uneconomical and impractical to place sensors on all spans as some are affected by weather conditions worse than others [9, 10]. Consequently, there have been several attempts to model the strategic placement of sensors and these are discussed next.

The placement of DTR sensor in its most primitive form is unsupervised and critical spans are selected by spacing the number of sensors evenly along the transmission line. This placement method is known as an 'equidistant placement' (EDP) strategy [11]. It works by defining the number of required sensors, n, and spacing them equally according to the simple rule $No.\ of\ spans/n + 1$. Obviously, this method ignores the variability of weather conditions and requires a large number of sensors in order to be useful. Hence, there have been several supervised placement strategies that give monitoring priority to those spans that are affected by less desirable weather conditions [12–14]. Under this condition, decisions are made based on expert knowledge and 'rule-of-thumb' unwritten rules. For example, spans sheltered from wind are suitable candidates for sensor placement. This approach, although useful, can quickly escalate into an unmanageable task as the number of spans increases indefinitely. Moreover, the decision made may vary among experts. The variability of opinions can also delay and confuse the decision-making process as conflicting suggestions are considered together. To make things worse, the stochastic nature of weather data makes it an even more difficult and complicated task.

To overcome the problem, there is a need for statistical modelling of DTR sensor placement. This approach has several advantages. First, it handles the stochasticity of weather data very effectively and can easily deal with situations involving a large number of spans. Besides that, it is also an objective-based process with no opinion bias. In this paper, the spans that are selected for monitoring are also known as the 'critical spans'.

To the authors' best knowledge, only Matus *et al.* [11] have taken this approach by proposing a heuristic to identify the critical spans for DTR sensor placement. In this paper, the minimum ratings derived from the critical spans and from all the spans were defined as 'DTRs' and 'actual ratings', respectively. Pearson's correlation between DTR and actual ratings was calculated and used as a benchmark to evaluate the performance of the algorithm. Hence, a higher correlation signifies a greater similarity between the two ratings and vice versa. Structurally, the algorithm began by selecting the first critical span that gave the highest correlation. Next, it selected an additional span that improved the correlation

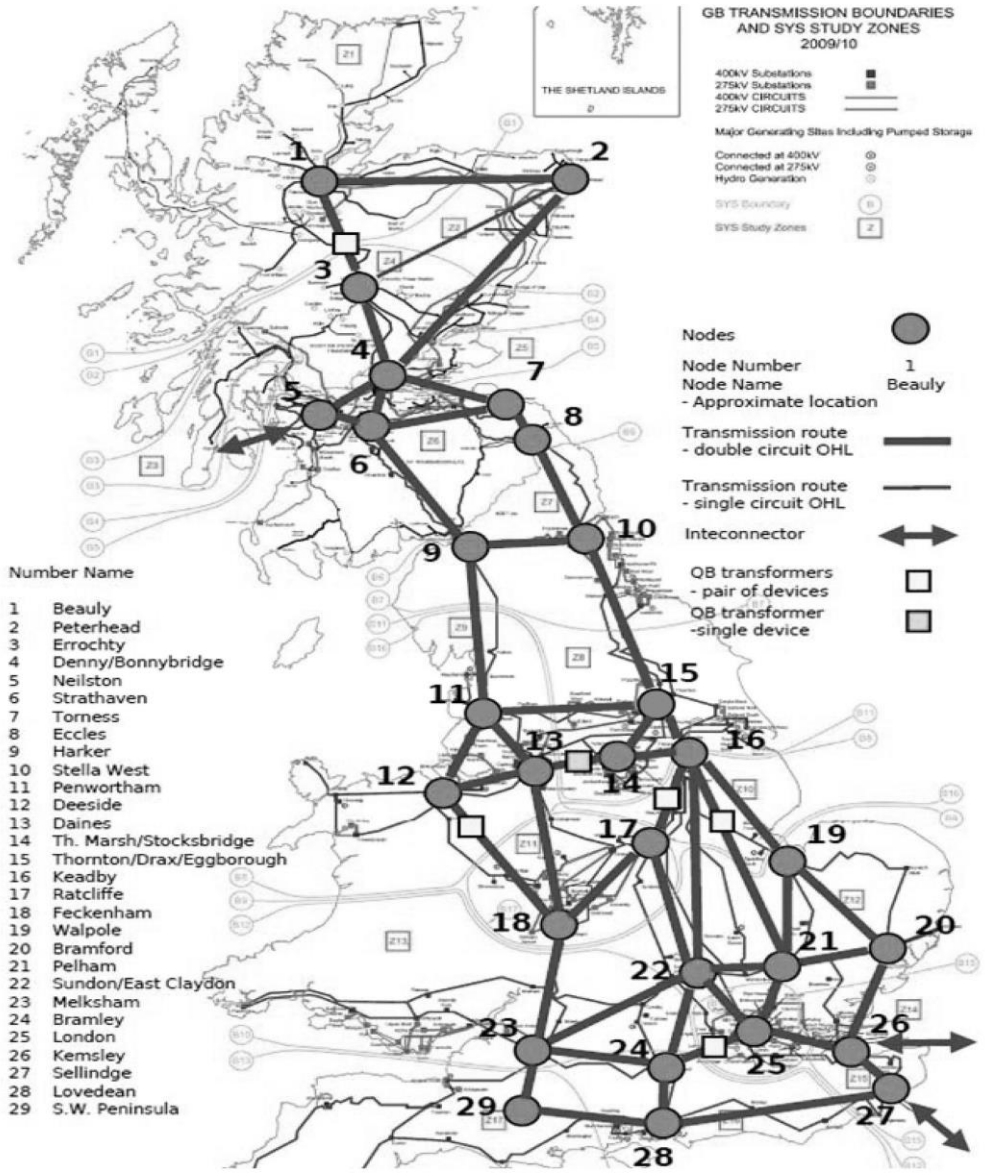

Fig. 1 *UK power transmission network and the portion connecting checkpoint 6-9-11-12-18*

the most and the process was repeated until the desired correlation benchmark was achieved.

Our investigations suggest that the algorithm considered only line thermal ratings during the identification of critical spans. The effects of DTRs on the spans' sagging levels are not considered. As the algorithm stopped at a certain correlation level and not all spans were monitored, it is possible that the derived DTRs are higher than the thermal capacity in some spans. Encountering such a situation can lead to excessive sag and ground clearance infringement. For this reason, sag is also a crucial component to consider when identifying the critical spans.

Therefore, this paper intends to fill this gap and proposes a new methodology for the identification of critical spans for DTR sensor placement. Our proposed methodology is unique as the identified critical spans provide DTRs that warrant no infringement of ground clearance in any spans, minimise sagging and are able to produce a high correlation with actual line ratings. To do this, our methodology was carried out in two phases. First, critical spans

were identified with the goal of avoiding ground clearance infringement due to excessive sag. Second, more spans were selected if the correlation of DTR and actual line ratings remained low or unsatisfactory. The second phase also ensures that the ageing effects of the conductor due to the exceedance of their maximum thermal limit are kept to the minimum.

Finally, the rest of this paper is arranged as follows. The set-up of the test system used to demonstrate the robustness of our identification model is laid out in Section 2. The proposed methodology for the identification of critical spans is presented in Section 3. Then, the performances of our proposed methodology are compared with the heuristic from [11] in Section 4. Finally, the conclusion is presented in Section 5.

2 Test system

2.1 Physical dimension

An overhead power line consisting of 70 tensioning sections was created and the number of spans in each section varied between 5 and 20 spans. The length of each span was randomly selected and was between 200 and 500 m. The additional allowable sag beyond the maximum design temperature (MDT) was assumed to be between 6 and 30 m. The spans with smaller ground clearance represent spans that might be hanging over trees, underground cables, hills, buildings, populated areas and so on. On the other hand, the spans with larger ground clearance are those normally hovering over valleys, unpopulated area and clear underpasses. In addition, all spans were strung with suspension insulators at 20% of their rated breaking strength in a temperature of 15°C. All the spans were also made with aluminium conductor steel reinforced (ACSR) Lapwing conductor. Finally, the length and weight of all suspension insulators were 5 m and 150 kg, respectively.

2.2 Weather data

Ten years of hourly historical weather data (wind speed, wind angle and ambient air temperature) from 25 weather stations located evenly along the line connecting checkpoint 6-9-11-12-18 as shown in Fig. 1 were collected from the BADC website [15].

These weather conditions were adopted into our test system and the positions of the stations were equally spaced along the test system. Hence, weather conditions from only 25 spans are known and the weather conditions in the remaining spans were derived using the inverse distance weighted (IDW) interpolation method [16]. IDW was chosen as it is the workhorse of spatial interpolation and is widely used by geographic information system (GIS) analysts [16]. It works according to Tobler's first law of geography and estimates unknown values as weighted averages over known values [17]. Mathematically, it is expressed as the following equation

$$Z_S = \frac{\sum_{i=1}^{n} z_i(1/d_i^k)}{\sum_{i=1}^{n}(1/d_i^k)} \tag{1}$$

where Z_S is the estimated weather value at span S. n is the total number of weather stations and is equal to 25 in this case. Z_i is the known weather value at span i where the weather station is located. d_i is the distance between span i and S. k is the specified power that determines the degree of control of local influence. $k=2$ is generally used by GIS analysts, although there is no theoretical justification for preferring this value. None the less, it has been shown that when $k=2$ is used, the stations located further away from the estimating point diminish in their influence [18]. Hence, $k=2$ is used in this paper.

3 Methodology

The proposed critical span identification model requires the calculation of conductor sag and line rating. Hence, the conductor sag model and line rating model are presented before explaining the proposed critical span identification model.

3.1 Conductor sag model

An overhead conductor attached to suspension insulator sets can move in the conductor's longitudinal and latitudinal directions. Most of the time, this movement is caused by the conductor's elongation, which in turn is affected by its length and the conductor's state change (normally affected by the conductor's temperature). Hence, the calculation of sag of a single span should consider these criteria.

However, a practical tensioning section normally consists of multiple spans with various lengths and they are affected by various weather conditions that influence their thermal profiles differently. Consequently, the elongation of one span will affect its neighbouring spans. As a result, a case with non-uniform conductor elongation across a tensioning section is normally presented. Therefore, all spans in a tensioning section should be considered simultaneously when determining their new sagging level due to conductor state change [19]. In solving this problem, the main objective is to determine the conductor's new horizontal tensile forces.

For a tensioning section with n spans, the new horizontal tensile force of each span is calculated as a multiple of its initial tensile force as shown in (2) [19] (see (2))

$$\begin{aligned}
&X_1^4\left[X_1K_{1,1}K_{2,1} - C_1(X_1, X_2)\right] \\
&+ \left(X_1K_{1,1} - \frac{EA}{H_0}\right)\left(X_1^2K_{3,1} + K_{4,1}\right)\frac{a_1^2}{L_{0,1}^2} = 0, \\
&\vdots \\
&X_i^4\left[X_iK_{1,i}K_{2,i} - C_i(X_{i-1}, X_i, X_{i+1})\right] + \left(X_iK_{1,i} - \frac{EA}{H_0}\right) \\
&\left(X_i^2K_{3,i} + K_{4,i}\right)\frac{a_i^2}{L_{0,i}^2} = 0, \\
&\vdots \\
&X_{n-1}^4\left[X_{n-1}K_{1,n-1}K_{2,n-1} - C_{n-1}(X_{n-2}, X_{n-1}, X_n)\right] \\
&+ \left(X_{n-1}K_{1,n-1} - \frac{EA}{H_0}\right)\left(X_{n-1}^2K_{3,n-1} + K_{4,n-1}\right)\frac{a_{n-1}^2}{L_{0,n-1}^2} = 0, \\
&X_n^4\left[X_nK_{1,n}K_{2,n} - C_n(X_{n-1}, X_n)\right] + \left(X_nK_{1,n} - \frac{EA}{H_0}\right) \\
&\left(X_n^2K_{3,n} + K_{4,n}\right)\frac{a_n^2}{L_{0,n}^2} = 0,
\end{aligned} \tag{2}$$

where

$$\begin{aligned}
K_{1,i} &= \left(1 + \bar{L}_{1,i}\right)\frac{L_{0,i}}{a_i}, \\
K_{2,i} &= -\left(1 + \bar{L}_{1,i}\right)^2\frac{L_{0,i}}{a_i} + \frac{EA}{H_0}\bar{L}_{1,i} + \frac{EA\varepsilon_t}{H_0}(1 + \bar{L}_{1,i})(T_2 - T_1), \\
K_{3,i} &= \frac{a_i^2}{24c^2}, \\
K_{4,i} &= \frac{a_i^4}{720c^4} - \left(\frac{a_i^2}{L_{0,i}^2}\cdot\frac{a_i^4}{1152c^4}\right), \\
\bar{L}_{1,i} &= \frac{a_i^2}{L_{0,i}^2}\left(\frac{a_i^2}{24c^2} + \frac{a_i^4}{720c^4}\right) - \left(\frac{a_i^4}{L_{0,i}^4}\cdot\frac{a_i^4}{1152c^4}\right),
\end{aligned}$$

$$C_i(X_{i-1}, X_i, X_{i+1}) = \frac{EAa_i}{H_0 L_{0,i}^2}\left\{\left[\frac{(X_{i+1}-X_i)L_{K,i+1}}{\sqrt{(G_{K,i+1}/H_0)^2+(X_{i+1}-X_i)^2}}\right]-\left[\frac{(X_i-X_{i-1})L_{K,i}}{\sqrt{(G_{K,i}/H_0)^2+(X_i-X_{i-1})^2}}\right]\right\} + \frac{EAh_i}{H_0 L_{0,i}^2}\left\{L_{K,i+1}\left[1-\frac{G_{K,i+1}/H_0}{\sqrt{(G_{K,i+1}/H_0)^2+(X_{i+1}-X_i)^2}}\right]-L_{K,i}\left[1-\frac{G_{K,i}/H_0}{\sqrt{(G_{K,i}/H_0)^2+(X_i-X_{i-1})^2}}\right]\right\},$$

$$c = (H_0/w)^2,$$

$$L_{0,i} = \sqrt{a_i^2+h_i^2},$$

$$G_{K,i} = \frac{J_{K,i}}{2} + X_{i-1}H_0\sinh[w(a_{i-1}+x_{A,i-1})/X_{i-1}H_0] - X_iH_0\sinh[wx_{A,i}/X_iH_0] \quad (2a)$$

where a is the span length, h is the difference in height of the conductor attachment, w is the weight per unit length of conductor, E is the conductor modulus of elasticity, A is the conductor cross-sectional area, L and J are the length and weight of the insulator, respectively, T is the conductor temperature, H_0 is the conductor's initial horizontal tensile force strung at 15°C, G_K is the equivalent vertical forces at the insulator set considering vertical loadings in adjacent spans and dead weight of the insulator and X_i is the multiplier of H_0 for span i.

From (2), determining X_i requires the knowledge of X_{i-1} and X_{i+1}. Hence, an explicit solution for each equation of (2) is not possible and it forms a system of n non-linear equations as shown in the following equation

$$\boldsymbol{f}(\boldsymbol{X}) = \begin{pmatrix} f_1(\boldsymbol{X}) \\ f_2(\boldsymbol{X}) \\ \vdots \\ f_n(\boldsymbol{X}) \end{pmatrix} = \begin{pmatrix} f_1(X_1, X_2, \ldots, X_n) \\ f_2(X_1, X_2, \ldots, X_n) \\ \vdots \\ f_n(X_1, X_2, \ldots, X_n) \end{pmatrix} = 0 \quad (3)$$

Using the Newton–Raphson approximation method, X_i is solved according to the following equation

$$\boldsymbol{X}_{\text{new}} = \boldsymbol{X}_{\text{old}} - \left[\boldsymbol{F}(\boldsymbol{X}_{\text{old}})\right]^{-1}\left(\boldsymbol{f}(\boldsymbol{X}_{\text{old}})\right) \quad (4)$$

$\boldsymbol{F}(\boldsymbol{X})$ is the Jacobian matrix and its element is found by partial derivation of X_i of vector $\boldsymbol{X}$. The partial derivative is shown in (5) and the Jacobian matrix is further expressed in (6).

$$f_{ik}(X_k) = \frac{\partial f_i(X_1, X_2, \ldots, X_n)}{\partial X_k} \quad (i, k = 1, 2, \ldots, n) \quad (5)$$

$$\boldsymbol{F}(\boldsymbol{X}) = \begin{pmatrix} f_{11}(X_1), & f_{12}(X_2), & \ldots, & f_{1n}(X_n) \\ f_{21}(X_1), & f_{22}(X_2), & \ldots, & f_{2n}(X_n) \\ \vdots & \vdots & \ldots, & \vdots \\ f_{n1}(X_1), & f_{n2}(X_2), & \ldots, & f_{nn}(X_n) \end{pmatrix} \quad (6)$$

For the same reason as $\boldsymbol{f}(\boldsymbol{X})$, explicit calculation of differential equation (5) is not possible. It is therefore approximated using the central difference method in the following equation:

$$f_{ik}(X_k) = \frac{f_i(X_k+h_k) - f_i(X_k-h_k)}{2h_k} \quad (7)$$

h_k is the suitably selected value of vector $\boldsymbol{h}$ and it dictates the step width of the Newton–Raphson iteration. In this paper, $h_k = 1$ is selected for all spans and the iteration is completed when the error of $\boldsymbol{f}(\boldsymbol{X})$ is less than 5%.

After the values of vector $\boldsymbol{X}$ have been found, the vector of the horizontal tensile force after temperature change, $\boldsymbol{H}_{\text{final}}$, is simply $\boldsymbol{X}H_0$. Finally, the sag at each span, S_i, is calculated as shown in the following equation

$$S_i = A \cdot B \cdot C \cdot D \cdot S_i^{\text{final}} \quad (8)$$

where

$$S_i^{\text{final}} = \frac{a_i^2(w)}{(8H_{\text{final}}^i)} \quad (8a)$$

The constants A, B, C and D can be obtained by referring to [19] on pages 562 and 563.

3.2 Line rating model

The steady-state thermal behaviour of a bare overhead line conductor can be described under the balance of its heat absorbing and releasing elements. These elements are identified by the IEEE 738 standard [4] as the convection heat loss, Q_c, radiated heat loss, Q_r, solar radiation heat gain, Q_s and joule heat gain, Q_j. These elements are in turn governed by the wind speed, V_w, its direction, ϕ, solar radiation angle, θ, ambient temperature, T_a, current flow, I, and the conductor resistance, R, as a function of the conductor operating temperature, T_c. The heating balance, HB, is achieved when these heating elements are summed to zero as expressed in the following equation:

$$\text{HB} = Q_j(I, R, T_c) + Q_s(\theta) - Q_r(T_c, T_a) - Q_c(T_c, T_a, V_w, \phi) = 0 \quad (9)$$

Specifically, the joule heat gain, Q_j, is calculated as in the following equation

$$Q_j = I^2R(T_c), \quad R(T_c) = \left[\frac{R(T_{\text{MDT}}) - R(T_{\text{min}})}{T_{\text{MDT}} - T_{\text{min}}}\right](T_c - T_{\text{min}}) + R(T_{\text{min}}) \quad (9a)$$

$R(T_{\text{MDT}})$ and $R(T_{\text{min}})$ are the conductor resistances at its maximum design temperature, T_{MDT}, and minimum temperature, T_{min}, respectively.

The solar radiation heat gain, Q_s, is calculated as in the following equation

$$Q_s = \lambda q_{se} \sin(\theta) A' \quad (9b)$$

λ is the solar absorptivity, q_{se} is the elevated corrected total solar and sky radiated heat flux rate and $A^{\wedge}$ is the projected area of the conductor per unit length.

The radiated heat loss, Q_r, is calculated as in the following equation

$$Q_r = 0.0178D\varepsilon\left[\left(\frac{T_c+273}{100}\right)^4 - \left(\frac{T_a+273}{100}\right)^4\right] \quad (9c)$$

D and ε are the conductor diameter and emissivity, respectively.

The convection heat loss, Q_c, is calculated as in (9d) if the wind speed is not zero

$$Q_{c1} = \left[1.01 + 0.0372\left(\frac{Dp_f V_w}{\mu_f}\right)^{0.52}\right] k_f K_{angle}(T_c - T_a)$$

$$Q_{c1} = \left[1.01 + 0.0372\left(\frac{Dp_f V_w}{\mu_f}\right)^{0.52}\right] k_f K_{angle}(T_c - T_a) \quad (9d)$$

$$K_{angle} = 1.194 - \cos(\phi) + 0.194\cos(2\phi) + 0.368\sin(2\phi)$$

$$Q_c = \max(Q_{c1}, Q_{c2})$$

where p_f, μ_f and k_f are the density, dynamic viscosity and thermal conductivity of air, respectively. If the wind speed is zero, Q_c is calculated as in (9e) instead

$$Q_c = 0.0205 p_f^{0.5} D^{0.75}(T_c - T_a)^{1.25} \quad (9e)$$

The conductor current is more conveniently expressed as (10) below by simple rearrangement of (9)

$$I = \sqrt{\frac{(Q_c + Q_r - Q_s)}{R(T_c)}} \quad (10)$$

The current flow is also used as the rating of the conductor. Hence, the maximum rating, I_{max}, is obtained when T_c is set as T_{MDT}. Hence a line section comprises many spans and all of them have different conditions, the ratings may differ from one span to another. Logically, the minimum rating among all the spans of a given line section is taken as the line rating for that section. This is officially shown in the following equation:

$$I_{max} = \min(I^1_{max}, I^2_{max}, \ldots, I^n_{max}) \quad (11)$$

n is the total number of spans in the considered section.

3.3 Critical span identification model

The process of identifying critical spans is carried out in two phases as explained below.

Phase 1: The objective of this phase is to identify the minimum number of critical spans in a tensioning section and its DTRs. When these ratings are applied to other non-critical spans that are from the same section, the violation of ground clearance should not occur. This minimisation issue is called the 'optimum sensor placement problem' (OSPP) and is formulated as (12) below

$$\text{OSPP}^{\Phi}_1: \min_{\forall i \in \boldsymbol{O}^{\Phi}} \sum_{i=1}^{n^{\Phi}} x^{\Phi}_{1,i}, \quad \Phi = 1, 2, \ldots, N$$
$$\text{s.t. } \Delta^{\Phi}_i = \varphi^{\Phi}_i - \psi^{\Phi}_i > 0 \quad (12)$$

In all of the symbols above, the subscript i and superscript Φ imply that they are referring to the ith critical span of the Φth tensioning section. This is also applicable to the rest of the paper unless otherwise stated. The symbol OSPP^{Φ}_1 refers to the first phase of OSPP, φ^{Φ}_i is the maximum allowable sag, ψ^{Φ}_i is the sagging level, Δ^{Φ}_i is the remaining sagging distance, n^{Φ} is the total number of spans, $\boldsymbol{O}^{\Phi}$ is the set of all spans and N is the total number of tensioning sections for the transmission line. Referring to the condition of subjectivity in (12), a positive value in Δ^{Φ}_i denotes no violation of ground clearance and vice versa. Finally, $x^{\Phi}_{1,i}$ is the binary decision variable of the first phase and is defined as

$$x^{\Phi}_{1,i} = \begin{cases} 1 & \text{if weather station is installed on span } i \\ 0 & \text{otherwise} \end{cases} \quad (12a)$$

Serving as the initialisation process in this phase, the span with the smallest ground clearance limit (allowable sags) in each tensioning section was selected as the first critical span

$$\text{Initialisation: } \boldsymbol{\kappa}^{\Phi} \leftarrow \min_{\forall i \in \boldsymbol{O}^{\Phi}} (\varphi^{\Phi}_i) \quad (12b)$$

The symbol $\boldsymbol{\kappa}^{\Phi}$ is the set of all currently identified critical spans. At this point, there is only one span in the set. However, more spans will be updated into it in later steps.

Next, a step-by-step explanation of this phase is given below:

(a) Deduce the DTRs of all the tensioning sections. This is performed by selecting the minimum rating from all the currently identified critical spans in each tensioning section as shown in (12c). The concept on which the equation is based is similar to (11).

$$\boldsymbol{R}^{\Phi} = \min_{\forall i \in \boldsymbol{\kappa}^{\Phi}} (\boldsymbol{I}^{\Phi}_i) \quad (12c)$$

$\boldsymbol{R}^{\Phi}$ is the vector of DTRs and $\boldsymbol{I}^{\Phi}_i$ is the set of rating vectors for all the currently identified critical spans in the set $\boldsymbol{\kappa}^{\Phi}$.

(b) Determine the effect of DTRs of each tensioning section, $\boldsymbol{R}^{\Phi}$, on the thermal profile of its remaining spans. This is performed using the iteration technique as shown in Fig. 2.

The technique works by back-calculating the conductor temperature, T^{Φ}_{ci}, of a particular span based on the ampacity flowing through the conductor and its surrounding weather conditions. The process converges when the heat balance error, $\text{HB}^{\Phi}_{\text{error }i}$, is found to be less than 0.01 W/m. Using a temperature resolution of 1°C, all T^{Φ}_{ci} exceeding the conductor maximum design temperature, $T^{\Phi}_{\text{MDT }i}$, are recorded. Hence, all temperatures with a resolution of less than 1°C are rounded off. This information is also accompanied by the average hourly duration of staying at those temperatures as 10 years of hourly weather data were used in the analysis. At the end, a temperature–duration pair matrix, $\mathbf{Y}^{\Phi}_i$, is produced for each span in all the tensioning

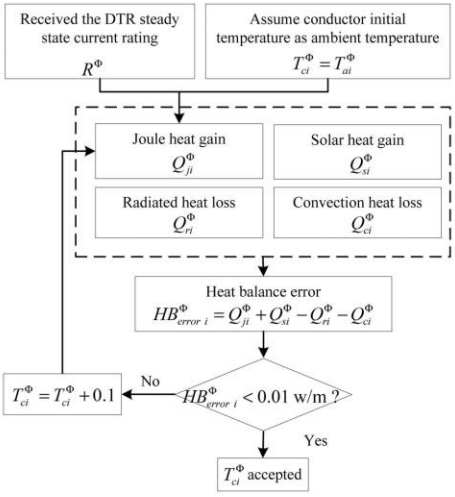

Fig. 2 *Iteration technique for back-calculate the conductor temperature*

sections and it has the form shown below

$$\mathbf{Y}_i^{\Phi} = \begin{bmatrix} T^{\Phi}_{\mathrm{MDT}\,i} + 1^{\circ}\mathrm{C} & T^{\Phi}_{\mathrm{MDT}\,i} + 2^{\circ}\mathrm{C} & \cdots & T^{\Phi}_{\mathrm{MDT}\,i} + n^{\circ}\mathrm{C} \\ t^{\Phi}_{1,i} & t^{\Phi}_{2,i} & \cdots & t^{\Phi}_{n,i} \end{bmatrix} \tag{12d}$$

$t^{\Phi}_{n,i}$ is the average duration of sustaining a temperature of $T^{\Phi}_{\mathrm{MDT}\,i} + n^{\circ}\mathrm{C}$.

(c) Calculate the equivalent final temperatures, $T^{\Phi}_{\mathrm{eq}\,i}$, for all the spans and the associated equivalent duration, $t^{\Phi}_{\mathrm{eq}\,i}$, of staying at $T^{\Phi}_{\mathrm{eq}\,i}$ based on the matrix $\mathbf{Y}_i^{\Phi}$. This is carried out using the Harvey annealing model [20] as shown in (12e) coupled with the technique described below

$$\mathrm{RS}^{\Phi}_{\mathrm{c}\,i} = \mathrm{RS}^{\Phi}_{\mathrm{al}\,i}\left(\frac{\mathrm{Str_{al}}}{\mathrm{Str_c}}\right) + 100 \times \left(\frac{\mathrm{Str_{st}}}{\mathrm{Str_c}}\right) \times 1.09 \tag{12e}$$

Such that

$$\mathrm{Str_c} = \mathrm{Str_{al}} + \mathrm{Str_{st}} = \frac{\pi}{4}(n_{\mathrm{al}} \cdot D^2_{\mathrm{al}} \cdot \mathrm{Sr_{al}} + n_{\mathrm{st}} \cdot D^2_{\mathrm{al}} \cdot \mathrm{Sr_{at}})$$

$$\mathrm{RS}^{\Phi}_{\mathrm{al}\,i} = \left(-0.24T^{\Phi}_{\mathrm{eq}\,i} + 134\right)\left(t^{\Phi}_{\mathrm{eq}\,i}\right)^{\left(0.095 - 0.001T^{\Phi}_{\mathrm{eq}\,i}(0.1/D_{\mathrm{al}})\right)}$$
$$\text{if } \left(-0.24T^{\Phi}_{\mathrm{eq}\,i} + 134\right) > 100, \quad \text{use } 100$$

All the parameters above with either the subscripts c, al or st mean that they are referring to the composite, aluminium and steel core of the ACSR conductor, respectively. RS is the percentage of remaining strength and Str is the calculated initial strength. Finally, n, D and Sr are the number, diameter and strength of the strands, respectively.

The step-by-step techniques used to carry out the Harvey model are

(1) Execute the Harvey model using the elements from the first column of matrix $\mathbf{Y}_i^{\Phi}$. At this stage, $T^{\Phi}_{\mathrm{eq}\,i}$ and $t^{\Phi}_{\mathrm{eq}\,i}$ in $\mathrm{RS_{al}}$ are the first and second elements from the first column of the matrix $\mathbf{Y}_i^{\Phi}$, respectively.
(2) While maintaining all the values calculated previously, replace $T^{\Phi}_{\mathrm{eq}\,i}$ with the temperature from the next column of matrix $\mathbf{Y}_i^{\Phi}$. However, $t^{\Phi}_{\mathrm{eq}\,i}$ is to be maintained as a variable and is solved by rearranging (12e). Then, the calculated $t^{\Phi}_{\mathrm{eq}\,i}$ is the equivalent duration of operating at this temperature.
(3) Repeat step (2) until the end of matrix $\mathbf{Y}_i^{\Phi}$.

Note that $t^{\Phi}_{\mathrm{eq}\,i}$ is currently not required in the remaining steps of the critical span identification algorithm, but it will be used in Section 4.3 later.

(d) Calculate the new horizontal tensile forces and sag levels of all the spans in all the tensioning sections based on their newly found $T^{\Phi}_{\mathrm{eq}\,i}$. This is performed using the conductor sag model as presented in Section 3.1 by substituting T_2 with $T^{\Phi}_{\mathrm{eq}\,i}$.
(e) Update the critical span set, $\boldsymbol{\kappa}^{\Phi}$, by selecting one of the remaining spans (within the same tensioning section) that displays the largest violation of ground clearance as below:

$$\text{Update:} \quad \begin{matrix} \boldsymbol{\kappa}^{\Phi} \leftarrow \min\limits_{\forall i \in \boldsymbol{\alpha}^{\Phi}} (\Delta_i^{\Phi} \,|\, \Delta_i^{\Phi} < 0) \\ \boldsymbol{\alpha}^{\Phi} = \boldsymbol{O}^{\Phi} - \boldsymbol{\kappa}^{\Phi} \end{matrix} \tag{12f}$$

$\boldsymbol{\alpha}^{\Phi}$ is the set of remaining spans after subtracting the currently selected critical span set, $\boldsymbol{\kappa}^{\Phi}$, from the set of all spans, $\boldsymbol{O}^{\Phi}$.

(f) The entire process is repeated from (a) to (e) for all the tensioning sections until no infringement of ground clearance occurs.

Phase 2: At the end of phase 1, some of the spans within a tensioning section will not be identified as critical. As a result, these remaining spans occasionally exceed their thermal limits due to them not being involved in determining the DTRs. However, for reasons of ground clearance adequacy, these spans also avoid the infringement of ground clearance and are not picked up in phase 1. Despite that, thermal overloads remain and accelerated ageing as a result of that is still inevitable in the affected spans. Hence, these spans should be identified as critical as well and be added into the pool of critical spans, $\boldsymbol{\kappa}^{\Phi}$.

Therefore, the objective of this phase is to identify the remaining critical spans and it is formulated as the minimisation problem stated below

$$\begin{aligned} &\mathrm{OSPP}_2^{\Phi}\text{: } \min_{\forall i \in \boldsymbol{\alpha}^{\Phi}} \sum_{i=\boldsymbol{\alpha}^{\Phi}(1)}^{\boldsymbol{\alpha}^{\Phi}(\mathrm{end})} x^{\Phi}_{2,i}, \quad \Phi = 1, 2, \ldots, N \\ &\text{s.t. } \rho = \mathrm{corr}(\boldsymbol{R}^{\Phi}, \Re^{\Phi}) \geq B \end{aligned} \tag{13}$$

OSPP_2^{Φ} refers to phase 2 of OSPP, $\Re^{\Phi}$ is the vector of actual ratings given that the actual minimum ratings at every hour are known, ρ is the Pearson's correlation between $\boldsymbol{R}^{\Phi}$ and $\Re^{\Phi}$ as shown in (13a), B is the targeted correlation benchmark and $x^{\Phi}_{2,i}$ is the variable decision in the second phase as defined in (13b). Finally, the rest of the notations are the same as mentioned previously

$$\rho = \frac{\sum_{h=1}^{H} (\boldsymbol{R}^{\Phi}_h - \overline{\boldsymbol{R}^{\Phi}_h})(\Re^{\Phi}_h - \overline{\Re^{\Phi}_h})}{\sqrt{\sum_{h=1}^{H} (\boldsymbol{R}^{\Phi}_h - \overline{\boldsymbol{R}^{\Phi}_h})^2 \sum_{h=1}^{H} (\Re^{\Phi}_h - \overline{\Re^{\Phi}_h})^2}} \tag{13a}$$

where H represents all the hourly ratings.

$$x^{\Phi}_{2,i} = \begin{Bmatrix} 1 & \text{if weather station is installed on the remaining span } i \\ 0 & \text{otherwise} \end{Bmatrix} \tag{13b}$$

As part of the continual process for the proposed methodology, the set of remaining spans, $\boldsymbol{\alpha}^{\Phi}$, the set of currently identified critical spans, $\boldsymbol{\kappa}^{\Phi}$, and the vector of DTRs, $\boldsymbol{R}^{\Phi}$, from phase 1 are inherited into phase 2 before further actions are taken.

Next, a step-by-step explanation of this phase is given below:

(a) Determine the Pearson's correlation value, ρ, according to (13a).
(b) Compare ρ with the benchmark value, B.
(c) Check for the following two possible outcomes and take the appropriate action.

Outcome 1: Given that B is not satisfied, $\boldsymbol{\kappa}^{\Phi}$ is updated by adding one of the remaining spans that improve ρ the most as shown below

$$\text{Update:} \quad \begin{matrix} \boldsymbol{\kappa}^{\Phi} \leftarrow \max\limits_{\forall i \in \boldsymbol{\alpha}^{\Phi}} (\rho_i) \\ \boldsymbol{\alpha}^{\Phi} = \boldsymbol{O}^{\Phi} - \boldsymbol{\kappa}^{\Phi} \end{matrix} \tag{13d}$$

ρ_i refers to the correlation value after adding one of the remaining spans as a critical span. Maximising the improvement of ρ ensures that the minimum number of additional spans is assigned as critical spans.
Outcome 2: Given that the benchmark is satisfied, phase 2 is considered done and marks the completion of the proposed methodology.

(d) The whole process is repeated from (a) to (c) until outcome 2 is met.

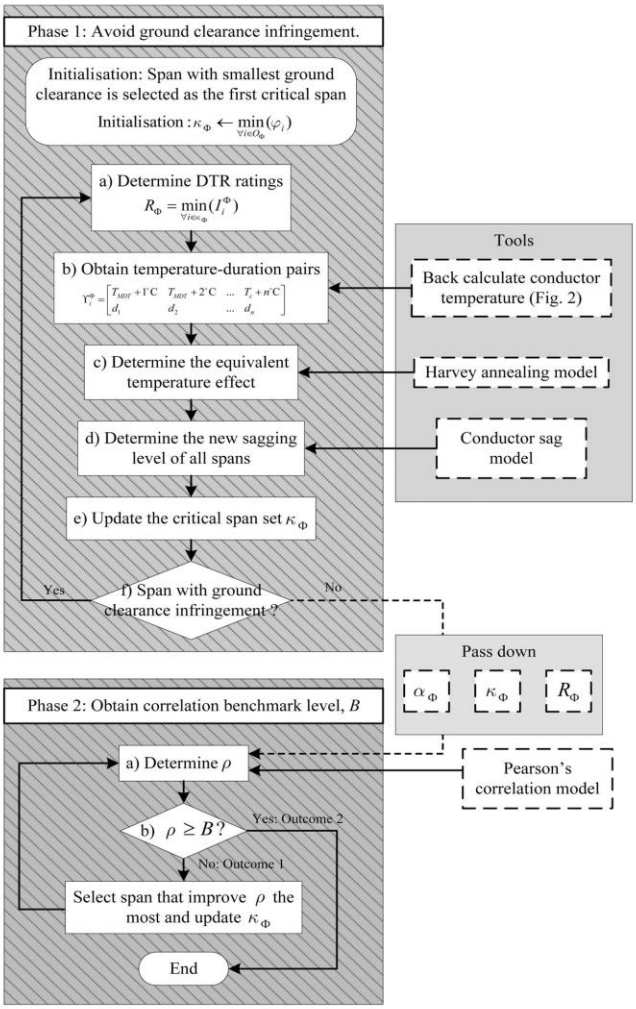

Fig. 3 *Proposed methodology for the identification of critical spans*

At the end of the methodology, after going through the first and second phases, $\boldsymbol{\kappa}^\Phi$ forms the final set of critical spans for all the tensioning sections. Finally, an illustration depicting the overview of the methodology is provided in Fig. 3.

4 Numerical results and discussions

Using the test system set up in Section 2, the critical span identification process was performed using the proposed methodology and the heuristic from [11]. In both of the techniques, the correlation benchmark was set at 99%.

4.1 Number of critical spans

First, the results from both of the techniques are compared from the perspective of the number of identified critical spans. The results of this analysis are shown in Fig. 4. It demonstrates that in most of the tensioning sections, the proposed methodology has more critical spans than the heuristic. In fact, in all cases, the heuristic has only one critical span. The results also show that the proposed methodology is able to pick up the critical spans that are otherwise not identified in the heuristic. The reason is because the proposed methodology considers sagging level and the correlation between DTR and actual line ratings. The heuristic, however, is only concerned with the correlation.

By considering additional yet important criteria, significant more critical spans are identified in the proposed methodology.

4.2 Sagging levels

In order to show that the larger critical span sets identified by the proposed methodology are necessary and superior to the heuristic, the remaining sagging distance, Δ_i^Φ, in all the spans was calculated. This was performed using the respective DTRs of the tensioning sections and the conductor sag model. After that, the

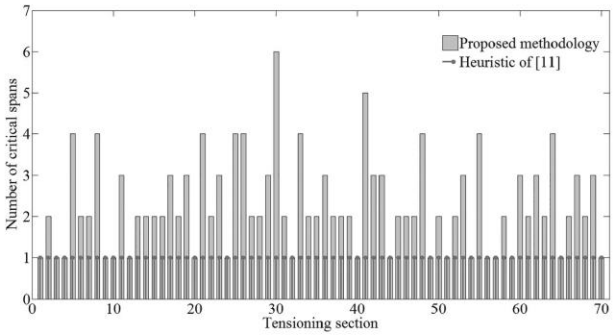

Fig. 4 *Number of critical spans identified by the proposed methodology and heuristic of [11]*

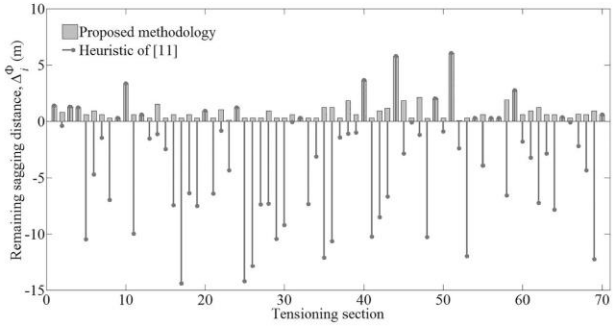

Fig. 5 *Remaining sagging distance based on the DTRs of the proposed methodology and the heuristic of [11]*

minimum of the remaining ground clearances in each tensioning section was determined. These results are shown in Fig. 5 and all the negative values indicate the amount of ground clearance infringement.

The results demonstrate that the proposed methodology ensures no violation of ground clearances in any of the tensioning sections. In contrast to that, the heuristic cannot provide the same warranty. In fact, most of the tensioning sections violate their maximum allowable sag as a result of deploying the heuristic.

Hence, the results prove that the larger critical span sets as given by the proposed methodology are indeed significant. In addition to that, the benefit of identifying critical spans based on the sagging limit, as given in phase 1 of the proposed methodology, has also been demonstrated.

4.3 Ageing effect of sensor placement

As it is impossible to place sensors on all the spans, it is inevitable that the DTRs are sometimes higher than the actual line ratings of the non-critical spans. In this situation, although the proposed methodology causes no violation of ground clearance, conductor ageing still takes place as a result of operating beyond the MDT. This section intends to quantify this ageing mechanism by introducing the expected life loss (ELL) index.

To do that, the IEEE 1283 standard [21] for describing the mean ageing value of a conductor at elevated temperature is examined and is provided below.

$$\varepsilon_{\mathrm{c}\,i}^{\Phi\mathrm{elv}} = 0.24(\mathrm{RS}_{\mathrm{c}\,i}^{\Phi})^{1.3}\left(T_{\mathrm{eq}\,i}^{\Phi}\right)^{1.4}\left(t_{\mathrm{eq}\,i}^{\Phi}\right)^{0.16} \tag{14}$$

$\varepsilon_{\mathrm{c}\,i}^{\Phi\mathrm{elv}}$ is the mean ageing value of a conductor as a result of operating at an elevated temperature beyond its MDT. $T_{\mathrm{eq}\,i}^{\Phi}$ and $t_{\mathrm{eq}\,i}^{\Phi}$ are determined from phase 1 of the proposed methodology as described previously.

However, if the conductors were able to operate at MDT all the time, annealing due to exceeding the MDT would be avoided and RS could be maintained at 100%. Under this condition, the equivalent duration, $t_{\mathrm{MDT}\,i}^{\Phi}$, needed to achieve $\varepsilon_{\mathrm{c}\,i}^{\Phi\mathrm{elv}}$ can be derived from (14) and is shown in the following equation

$$t_{\mathrm{MDT}\,i}^{\Phi} = \exp\left[\frac{\ln\left(\varepsilon_{\mathrm{c}\,i}^{\Phi\mathrm{elv}}/0.24(T_{\mathrm{MDT}\,i}^{\Phi})^{1.4}\right)}{0.16}\right] \tag{15}$$

Hence, the ELL of each span is calculated as the difference between $t_{\mathrm{MDT}\,i}^{\Phi}$ and $t_{\mathrm{eq}\,i}^{\Phi}$ as shown in the following equation

$$\mathrm{ELL} = t_{\mathrm{MDT}\,i}^{\Phi} - t_{\mathrm{eq}\,i}^{\Phi} \tag{16}$$

Following that, the ageing effects of all the spans as a result of deploying the DTR sensors according to the proposed methodology and the heuristic of [11] were determined by calculating their ELL indexes. Then, the ELL indices of all the spans from the same tensioning section were consolidated by taking the median among them and the results are shown in Fig. 6.

The figure shows a comparison of the ELL indices between the proposed methodology and the heuristic of [11]. It clearly shows that the ELL indices of the proposed methodology are much lower than those given by the heuristic. This also means that there are fewer occasions of conductor thermal overload when the DTR sensors are placed according to the methodology. Hence, from the ageing effect perspective, the proposed methodology is also far superior to the heuristic of [11].

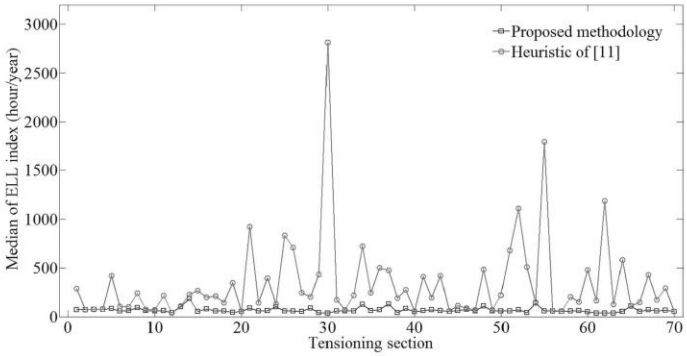

Fig. 6 *Comparison of the median ELL values of all tensioning sections after employing the proposed methodology and the heuristic of [11]*

5 Conclusion

This paper presented a methodology for the identification of critical spans for DTR sensor placement by considering the sagging limit and the correlation of DTRs with actual line ratings. The methodology is divided into two parts. First, it finds the critical spans that are required to produce the DTRs that can avoid ground clearance infringement in all spans. Second, in order to reduce the ageing effects induced by the DTRs, further critical spans are identified until the desired correlation benchmark is achieved.

The proposed methodology was compared with the heuristic of [11]. For a fair comparison, a test system that resembles real-life scenarios was set up and its weather data was obtained from the historical record found on the BADC website. Both of the algorithms were implemented on the test system and their performances were examined from three perspectives: the number of critical spans, sagging levels and ageing effects.

When the number of the identified critical spans is compared, the heuristic manages to identify fewer critical spans than the proposed methodology. However, this is not a good indication that the heuristic is the better performing algorithm of the two. This remark is backed by the results examined from the sagging level and ageing effect perspectives. The results show that the proposed methodology manages to avoid ground clearance infringement while the heuristic does not. In addition, the proposed methodology also produces fewer ageing effects than the heuristic. Therefore, it is concluded that the proposed methodology manages to outperform the heuristic in [11].

Finally, as mentioned previously in Section 1, selecting critical spans based solely on expert opinions and judgments can be a daunting and confusing task. This problem can be alleviated by incorporating the proposed methodology when identifying the critical spans in the DTR system planning process. Depending on the DTR system planner, the critical spans given by the proposed methodology can be taken as the first draft or the final result. If the DTR system planners choose to validate the result further, expert opinions can be used to modify and enhance results. This method is faster, easier and far more manageable than trying to identify the critical spans from scratch. Otherwise, the results given by the proposed methodology can be taken as they are.

6 Acknowledgments

The authors thank the Universiti Sains Malaysia (USM) and the Ministry of Higher Education Malaysia (MOHE) for the funding support.

7 References

1 Davis, M.W.: 'A new thermal rating approach: the real time thermal rating system for strategic overhead conductor transmission lines – Part I: General description and justification of the real time thermal rating system', *IEEE Trans. Power Appar. Syst.*, 1977, **96**, pp. 803–809
2 Seppa, O., Clements, M., Damsgaard-Mikkelsen, S., *et al.*: 'Application of real time thermal ratings for optimizing transmission line investment and operating decisions'. CIGRE Paper 22-301, 2000
3 'Increasing Capacity of Overhead Transmission Lines: Needs and Solutions', *Cigre Brouchure*, 2010
4 'IEEE Standard for Calculating the Current-Temperature of Bare Overhead Conductors', *IEEE Std 738-2006 (Revision of IEEE Std 738-1993)*, 2007, pp. c1–59
5 Seppa, T.O.: 'Increasing transmission capacity by real time monitoring'. IEEE Power Engineering Society Winter Meeting, 2002, 2002, vol. 2, pp. 1208–1211
6 Howington, B.S., Ramon, G.J. 'Dynamic thermal line rating summary and status of the State-of-the-art technology', *IEEE Trans. Power Deliv.*, 1987, **2**, (3), pp. 851–858
7 Yi, Y., Lambert, F., Divan, D.: 'A survey on technologies for implementing sensor networks for power delivery systems'. IEEE Power Engineering Society General Meeting., 2007, pp. 1–8
8 Muhr, M., Pack, S., Jaufer, S.: 'Usage and benefit of an overhead line monitoring system'. Int. Conf. on High Voltage Engineering and Application (ICOHVE), 2008, pp. 557–561
9 Shaker, H., Fotuhi-Firuzabad, M., Aminifar, F.: 'Fuzzy dynamic thermal rating of transmission lines', *IEEE Trans. Power Deliv.*, 2012, **27**, pp. 1885–1892
10 Shaker, H., Zareipour, H., Fotuhi-Firuzabad, M.: 'Reliability modeling of dynamic thermal rating', *IEEE Trans. Power Deliv.*, 2013, **28**, pp. 1600–1609
11 Matus, M., Saez, D., Favley, M., *et al.*: 'Identification of critical spans for monitoring systems in dynamic thermal rating', *IEEE Trans. Power Deliv.*, 2012, **27**, pp. 1002–1009
12 Black, J., Connor, S., Colandairaj, J.: 'Planning network reinforcements with dynamic line ratings for overhead transmission lines'. 45th Int. Universities Power Engineering Conf. (UPEC), 2010, 2010, pp. 1–6
13 Callahan, P.M., Douglass, D.A.: 'An experimental evaluation of a thermal line uprating by conductor temperature and weather monitoring', *IEEE Trans. Power Deliv.*, 1988, **3**, pp. 1960–1967
14 Pytlak, P., Musilek, P.: 'An intelligent weather-based system to support optimal routing of power transmission lines'. IEEE Electric Power and Energy Conf. (EPEC), 2010, 2010, pp. 1–6
15 B. A. D. C. (BADC). Available at: http://www.badc.nerc.ac.uk/home/
16 Eldrandaly, K.A., Abu-Zaid, M.S.: 'Comparison of six GIS-based spatial interpolation methods for estimating air temperature in western Saudi Arabia', *J. Environ. Inf.*, 2011, **18**, pp. 851–858
17 Longley, P., Goodchild, M., Maguire, D., *et al.*: 'Geographic information systems and science' (Wiley, New York, 2011)
18 *ArcGIS Resources Centre*. Available at: http://www.help.arcgis.com/en/arcgisdesktop/10.0/help/index.html#//00310000002m000000
19 Kiessling, F.: 'Overhead power lines: planning, design, construction' (Springer, 2003)
20 Harvey, J.R.: 'Effect of elevated temperature operation on the strength of aluminum conductors', *IEEE Trans. Power Appar. Syst.*, 1972, **PAS-91**, pp. 1769–1772
21 'IEEE Approved Draft Guide for Determining the Effects of High Temperature Operation on Conductors, Connectors, and Accessories', *IEEE P1283/D8, April 2013*, 2013, pp. 1–39